Proceedings of the ASME 2016 35th International Conference on Ocean, Offshore and Arctic Engineering
OMAE2016
June 19 - 24, 2016, Busan, Korea

OMAE2016-54437

REAL-TIME HYBRID MODEL TESTING OF A BRACELESS SEMI-SUBMERSIBLE WIND TURBINE. PART II: EXPERIMENTAL RESULTS

Erin E. Bachynski
MARINTEK
7450 Trondheim, Norway

Maxime Thys*
MARINTEK
7450 Trondheim, Norway

Thomas Sauder
MARINTEK
7450 Trondheim, Norway
NTNU AMOS / IMT
7491 Trondheim, Norway

Valentin Chabaud
NTNU / IMT
7491 Trondheim, Norway

Lars Ove Sæther
MARINTEK
7450 Trondheim, Norway

ABSTRACT

Real-Time Hybrid Model (ReaTHM) tests of a braceless semi-submersible wind turbine were carried out at MARINTEK's Ocean Basin in 2015. The tests sought to evaluate the performance of the floating wind turbine (FWT) structure in environmental conditions representative of the Northern North Sea. In order to do so, the tests employed a new hybrid testing method, wherein simulated aerodynamic loads were applied to the physical structure in the laboratory. The test method was found to work well, and is documented in [1].

The present work describes some of the experimental results. The test results showed a high level of repeatability, and permitted accurate investigation of the coupled responses of a FWT, including unique conditions such as blade pitch faults. For example, the influence of the wind turbine controller can be seen in decay tests in pitch and surge. In regular waves, aerodynamic loads due to constant wind had little influence on the structure motions (except for the mean offsets). Tests in irregular waves with and without turbulent wind are compared directly, and the influence of the wave-frequency motions on the aerodynamic damping of wind-induced low-frequency motions can be observed.

*Corresponding author: maxime.thys@marintek.sintef.no

INTRODUCTION

Floating wind turbines (FWTs) are an emerging technology which can be used to generate electricity from the significant wind resource in relatively deep water (>50 m). Scaled model tests are an important part of the qualification process for such novel concepts, and such tests may have many different objectives. Model tests can, for example, be used to confirm system behavior, evaluate nonlinear phenomena, assess extreme and detailed loads, validate computer codes, or convince decision makers of the feasibility of a concept [2].

There are, however, significant challenges related to carrying out scaled model tests of FWTs in an ocean basin. Hydrodynamic tests generally follow Froude scaling, but a consistent scaling of the wind turbine will then result in a reduced Reynolds number compared to the prototype, which leads to generally poor aerodynamic performance [3]. Furthermore, there are practical challenges related to generating (and measuring) constant and turbulent wind fields in a wave basin [4, 5].

In order to improve the aerodynamic load modeling in wave basin experiments, several researchers have attempted various forms of "non-geometrical" scaling of the wind turbine rotor. One form of non-geometrical scaling is to replace the wind turbine rotor with a drag disk (e.g. [6, 7]), which gives the correct mean thrust and provides some aerodynamic damping, and

can provide gyroscopic forces if spinning. A more sophisticated method of non-geometrical scaling is to modify the wind turbine airfoil shape and chord length in order to obtain improved performance at low Reynolds numbers. Improvements to the turbine performance in a wave basin have been documented, but it is not currently possible to simultaneously match the thrust, torque, and slope of the thrust curve adequately [8–10]. Numerical code validation using tests with non-geometrically scaled rotors has also proved challenging due to three-dimensional effects at low Reynolds numbers which are not accounted for by commonly used methods such as blade/element momentum [11].

In addition to the torque and thrust, accurate modeling of other aerodynamic forces and moments (such as the sway force and yaw moment), including the effects of the wind turbine control system, may be important. When the experimental goal is to qualify the global performance of the system, a so-called "real-time hybrid model testing" approach may be applied: in the case of the FWT in the wave basin, this implies that the aerodynamic forces are actuated upon the physical model according to simultaneous (real-time) simulations of the turbine rather than being generated by a small-scale physical turbine [1,12–14]. Real-time hybrid model testing will be referred to as ReaTHM^{TM} testing (a trademark of MARINTEK) in the following. The platform motions are measured and passed to the numerical simulator, and actuators apply appropriate aerodynamic/generator forces and moments based on the results of the numerical simulations.

Basin tests of FWTs with hybrid test techniques are relatively new, and previous tests have focused solely on the application of the thrust force [12]. The test campaign for NOWITECH extends the ReaTHM testing concept to 5 degree-of-freedom aerodynamic/generator loads, at a larger scale than previously tested, using a novel actuation system.

The objectives of the test campaign were twofold: 1) to quantify the system behaviour in environmental conditions representative of the Northern North Sea, and 2) to prove the applicability of the hybrid test method. In addition, the results from these tests are expected to be used to validate numerical hydrodynamic and structural models of floating offshore wind turbines. Extensive documentation tests as well as several potentially design-driving load cases with turbulent wind, irregular waves, and current were therefore carried out.

The test method is documented in Part I [1], while this work provides details of the test set-up and presents some of the interesting findings from the model test campaign. Calibration of a numerical model of the floating wind turbine is described in Part III [15].

MODEL DESCRIPTION

The 5MW CSC platform, which supports the NREL 5MW wind turbine, was selected for testing [16, 17]. The physical model comprises the hull, tower, and rotor-nacelle-assembly (RNA) model for the hybrid test method. The Froude scaling law was applied based on a linear scale factor of $\lambda = 30$, and all values given in this paper are given in prototype (full) scale unless otherwise noted. The basin floor was positioned at a depth of 6.66 m which corresponds to a prototype scale depth of 200 m.

Coordinate systems

As shown in Fig. 1, the global Earth-fixed coordinate system is located at the centerline of the tower at the waterline at the platform's resting static position. The z axis of the global coordinate system points downward and the system coincides with the location where waves were measured during calibration. This system is offset from the geometric center of the basin (extents shown in pink).

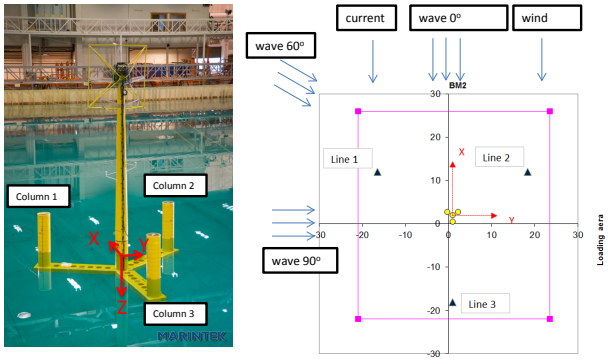

FIGURE 1. VIEW OF THE PHYSICAL MODEL AND GLOBAL COORDINATE SYSTEM

Hull

The hull of the CSC platform includes three side columns, three pontoons, and a central column, as described in Table 1.

TABLE 1. HULL GEOMETRY

Draft	30	m
Central column diameter	6.5	m
Side column diameter	6.5	m
Pontoon height	6.0	m
Pontoon width	9.0	m
Central column freeboard	10.0	m
Side column freeboard	20.0	m
Center-to-center (central to side column)	41.0	m
Center-to-edge (central column to pontoon end)	45.5	m

The main material used for manufacturing the model is alu-

minum and CNC-cut Divinycell foam with a ground and painted surface. The model was ballasted with solid weights. The mass, centre of gravity (CoG), and mass moment of inertia in pitch and yaw were calibrated by weighing and by performing oscillation tests in air with the model in a cradle. Hollow columns and ballasting compartments were included to allow for adjustable and accurate ballasting of the structure.

The measured mass and inertia characteristics of column 3 are given in Table 2. Note that the vertical center of gravity (VCG) is given in the basin coordinate system (positive z downward). Relatively large deviations in the mass and inertia were permitted for this part of the structure. The measured mass and inertia of the complete structure is described in Table 4.

TABLE 2. MASS CHARACTERISTICS OF COLUMN 3

	Specified	Measured	Deviation
Mass (tonnes)	435	456.7	5 %
VCG (m)	10.938	12.93	18.21 %
I_{yy} own CG (tonne-m^2)	81017	96093	18.61 %
I_{zz} own CG (tonne-m^2)	2193	-	-

Tower and RNA

The tower and RNA were designed to be as rigid as possible and to match the mass characteristics of the NREL 5MW wind turbine [17] with the OC3-Hywind tower design [18]. The dimensions of the frame were designed to accommodate the hybrid test system, within the dimensional limits dictated by the mass and stiffness specifications. Although rather poor agreement in the local I_{yy} can be observed, the deviation was found to be acceptable, since there is little effect on the overall system properties.

TABLE 3. MASS CHARACTERISTICS OF TOWER AND RNA

	Specified	Measured	Deviation
Mass (tonnes)	598.6	714.0	19.2 %
VCG (m)	70.48	58.23	17.38 %
I_{yy} own CG (tonne-m^2)	447244	978590	118.8 %
I_{zz} own CG (tonne-m^2)	16328	-	-

Combined Hull, Tower and RNA

The measured dry mass characteristics of the complete model (excluding the mooring system) are shown in Table 4. As shown, the overall platform was approximately 5 % lighter than the specification, however the mass moment of inertia in pitch was approximately 1.5 % higher than specified.

TABLE 4. MASS CHARACTERISTICS OF COMPLETE MODEL

	Specified	Measured	Deviation
Mass (tonnes)	10214.5	9730	4.7%
VCG (m)	18.9	19.05	0.79 %
I_{yy} about CG (tonne-m^2)	10157700	10297582	1.38 %
I_{zz} about CG (tonne-m^2)	8054160	7641621	5.12 %

Mooring System

The mooring system of the 5MW CSC wind turbine consists of 3 catenary mooring lines. The mooring system was built to match the weight characteristics of the lines in water, but the axial stiffness of the mooring lines was not considered in the scaling (as this stiffness was found to have insignificant influence on the restoring properties for the offsets of interest). The mooring system layout is described in Table 5 and Fig. 1.

TABLE 5. MOORING SYSTEM LAYOUT, REFERRED TO GLOBAL COORDINATE SYSTEM

	Fairlead			Anchor		
	x (m)	y (m)	z (m)	x (m)	y (m)	z (m)
Line 1	22.98	-39.8	27.0	301.5	-522.2	200
Line 2	22.98	39.8	27.0	301.5	522.2	200
Line 3	-45.95	0.0	27.0	-603.0	0.0	200

As per the prototype design, the mooring lines consist of two chain segments with no clump weights. For the model test, the mooring lines were made from chain with lead wires added for weight correction. Table 6 summarizes the mass and wetted weight of the mooring line segments as built. The diameter is given according to the specification: for simulations, the axial stiffness is assumed to be determined by a circular cross-section with the given diameter and Young's modulus of $E = 6.3 * 10^9$ kN/m^2. That is, the as-built mooring system has higher axial stiffness when scaled than the specified prototype ($E = 2.1 * 10^8$ kN/m^2).

TABLE 6. MOORING LINE CHARACTERISTICS AS BUILT

Segment	Length (m)	Mass per length (kg/m)	Wet weight (kN/m)	Spec. diameter (m)
Upper	240.00	235.0	2.005	0.195
Lower	367.55	446.0	3.804	0.269

Aerodynamic Load Model

The aerodynamic load calculations were carried out in a Fortran Dynamic Link Library (DLL) which calls the open source

code AeroDyn v13.00.01a-bjj [19]. AeroDyn [20] is a well-known implementation of the blade element/momentum (BEM) and generalized dynamic wake (GDW) methods, which has been validated against experimental data [21]. BEM was applied for mean wind speeds of 8 m/s, while GDW was applied for all other wind speeds.

As described in greater detail in Part I [1], the aerodynamic and generator loads were calculated using AeroDyn and the "Bladed-style" DISCON controller defined for the OC3 study, with some modifications for cases where blade pitch fault or shutdown are to be included. The aerodynamic calculations are carried out in full scale, with the measured positions, orientations, and velocities, as well as the applied loads, scaled according to Froude scaling.

INSTRUMENTATION

The measured responses during the tests included the platform motions and accelerations at the nacelle, wind turbine rotational speed, total aerodynamic and generator loads on the rotor, sectional moments and shear forces at the base of the tower and at the base of column 3, and mooring line tensions at the fairleads. A single ultra-thin instrumentation and power cable (under the model) was used. During wave calibration, wave elevations were sampled at 200 Hz in model scale. During the tests with the model, wave and force measurements were sampled at 600Hz in model scale.

The wave elevation was measured using conductance-type wave probes. Three probes were used during calibration, while only one was kept during tests with the model. The current speed was measured during calibration using acoustic time travel difference.

The forces on the mooring lines were measured using 280 N ring-type force transducers located at the upper end of each mooring line.

Bending moments and shear forces were measured at the base of the tower (10 m above the still water level) and at the base of the back column (column 3, at the point where the column meets the pontoon, at a depth of 24 m). Four strain gauges on the tower and four strain gauges on the column were used.

Several systems were in place to measure the motions and accelerations of the model. The motions of the vessel were measured by the OQUS position measuring system which is an optical-electronic system. Four (4) passive (reflective) diodes on the tower of the model and onshore cameras were employed. Translational accelerations were measured using an accelerometer in the nacelle of the model. Rates of rotation were measured using a gyrometer in the nacelle. The OQUS measurements were sampled at 100 Hz.

The approximate measurement accuracies are given in Table 7 in model scale. The OQUS accuracies refer to dynamic resolution.

TABLE 7. MODEL SCALE MEASUREMENT ACCURACIES

OQUS x-,y- and z-motions	0.5 mm
OQUS roll, pitch and yaw	0.05 deg
Wave probes	1.0 mm
Current speed	5 mm/s
Force transducers	2 % of meas. value for sign. resp. levels

TEST PROGRAM

The complete test program was designed to include identification tests, with and without the hybrid system, as well as deterministic (regular, constant) and random (irregular, turbulent) wave and wind tests. Two tests were carried out with wind, wave, and current, and several tests were carried out with the wind turbine in a fault condition.

PULLOUT TESTS

After installation of the model and connection of the mooring system, the draft and pretension were measured and checked. Pullout tests were then carried out to check the static restoring force and tensions of the mooring system. The results of the pull-out tests are provided in Tables 8-9. The tabulated data includes the offset (η), total restoring force or moment from the mooring system (F_r), and the tension in the mooring line with maximum tension (T_{max}).

All offsets are based on the motion at the waterline (ie, in the global Earth-fixed coordinate system). As expected, the mooring system is more stiff in +x than in -x.

TABLE 8. PULL-OUT TESTS IN SURGE

-x			+x		
η	F_r (kN)	T_{max} (kN)	η	F_r (kN)	T_{max} (kN)
0.00	0	1595	0.00	0	1595
2.52	240	1680	1.03	110	1671
3.88	363	1732	2.60	282	1794
7.09	644	1856	5.05	571	2008
9.34	832	1948	10.61	1340	2644
12.18	1066	2080	15.31	2212	3426
14.95	1305	2223	19.84	3479	4635
			24.19	5020	6148

DECAY TESTS

Decay tests were carried out to establish the natural periods and damping of the rigid body modes of motion. Decay tests in all six degrees of freedom were carried out in calm water without wind, and decay tests in surge and pitch were carried out for wind speeds below, at, and above the rated wind speed. The

TABLE 9. PULL OUT TESTS IN SWAY AND YAW

+y			+yaw		
η	F_r (kN)	T_{max} (kN)	η	F_r (kNm)	T_{max} (kN)
0.00	0	1595	0.00	0	1595
0.97	94	1654	0.37	2221	1596
2.26	225	1736	2.68	9061	1603
4.99	494	1916	4.78	15940	1613
7.86	780	2124	7.12	23672	1625
10.67	1020	2306			
13.29	1285	2526			

natural periods of the model in various configurations are summarized in Table 10. The hybrid system is active in all of the tests presented here; see [1] for an evaluation of the performance of the hybrid system. The wind turbine control system is active in all simulations with nonzero wind.

TABLE 10. NATURAL PERIODS FROM DECAY TESTS

Motion	No wind loads	8 m/s	11.4 m/s	15 m/s
Surge (s)	86.1	90.3	94.2	90.5
Sway (s)	85.3	-	-	-
Heave (s)	25.5	-	-	-
Roll (s)	28.3	-	-	-
Pitch (s)	29.2	30.5	36.5	32.2
Yaw (s)	59.4	-	-	-

The mean offsets of the platform in constant wind can also be obtained from the decay tests with wind, as given in Table 11. The mean offset is subtracted from all subsequent figures, such that the results can more easily be compared to the tests without wind forces.

TABLE 11. MEAN OFFSETS IN CONSTANT WIND

Motion	8 m/s	11.4 m/s	15 m/s
Surge (m)	-4.75	-7.6	-4.0
Pitch (deg)	3.45	5.4	3.0

Damping values are presented as a function of the amplitude of motion. The ratio of damping compared to critical damping (ζ^*) is calculated based on the logarithmic decrement (δ) for each cycle:

$$\delta = \ln \frac{x_n}{x_{n+1}} \tag{1}$$

where x_n and x_{n+1} are two consecutive peaks or troughs. The damping ratio is then found as:

$$\zeta^* = \frac{1}{\sqrt{1+(\frac{2\pi}{\delta})^2}}. \tag{2}$$

In some cases, and especially for small motion amplitudes, there are large variations in the damping level.

Decay tests below rated wind speed

Four decay tests in surge and three decay tests in pitch were carried out with 8 m/s constant wind.

The surge decay results with 8 m/s constant wind are compared to the tests with zero wind forces in Figs. 2 and 3. Note that some tests were initiated with positive surge, while others were initiated with a negative surge displacement, and multiple iterations (it. in the figure) are shown. Compared to the tests without wind, a slight increase in damping is observed, but this increase is relatively small due to the low velocity at the nacelle. Nonetheless, a significant lengthening of the natural period (5 seconds) is observed due to the wind forces, including the action of the torque controller.

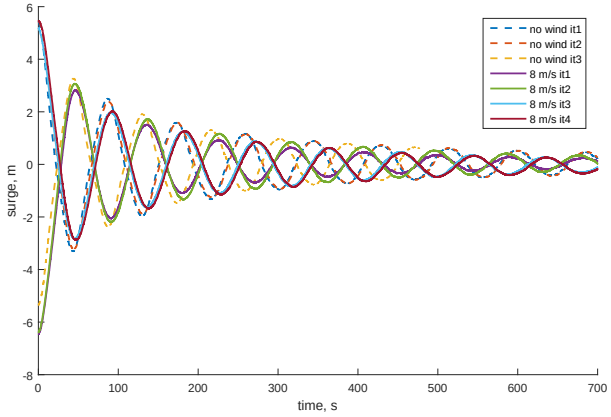

FIGURE 2. SURGE DECAY, 8 m/s CONSTANT WIND

Fig. 4 shows the pitch decay tests with below-rated wind speed. As expected, there is significant aerodynamic damping in pitch. Since the natural period in pitch is smaller than in surge, and the excursions at the nacelle are larger, the relative velocity is higher in the pitch decay test than in the surge decay test.

Fig. 4 also shows that the natural period is longer for the platform in below-rated wind speed than without wind. There is, however, significant variation in the length of each cycle, and some variation from test to test. The natural period tends to lengthen for later cycles.

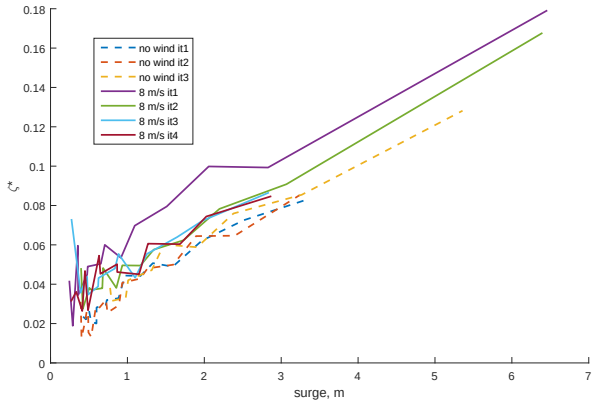

FIGURE 3. SURGE DAMPING, 8 m/s CONSTANT WIND

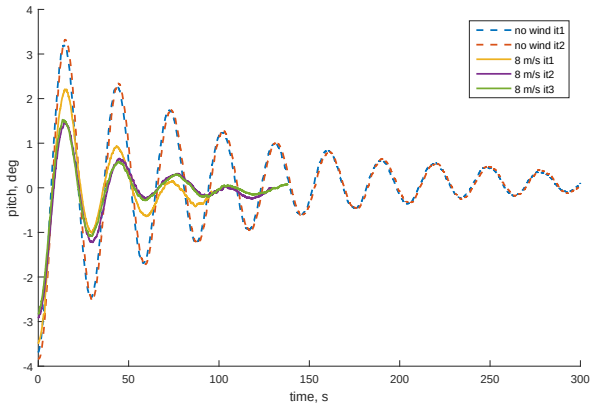

FIGURE 4. PITCH DECAY, 8 m/s CONSTANT WIND

Decay tests at rated wind speed

Next, four surge and three pitch decay tests were carried out for 11.4 m/s wind speed, which corresponds to the rated wind speed for the NREL 5 MW wind turbine [17]. The platform motions during the decay tests are shown together with the blade pitch angle in Fig. 5 and 7.

During the surge decay tests at rated wind speed (Fig. 5), a limit cycle in the motions was reached. The reason for the limit cycle behavior is related to the blade pitch controller in the wind turbine. The PI controller for blade pitch is tuned such that the controller natural frequency is 0.2 rad/s, which is slightly below the pitch natural frequency, but above the surge natural frequency [18,22]. This means that the blade pitch controller is able to react to the relative velocity in surge and a negative feedback mechanism is in place: as the platform moves toward the wind, the blade pitch increases due to the increase in rotational speed, and the thrust decreases - allowing the platform to oscillate further. Similarly, as the platform moves with the wind, the blade pitch decreases.

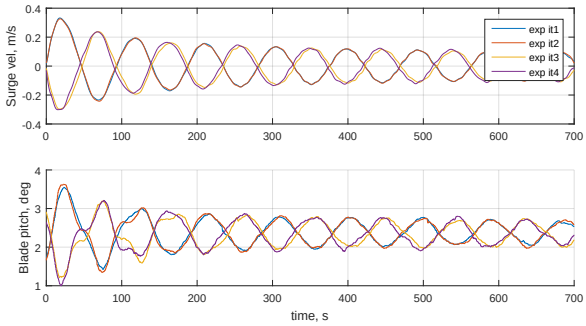

FIGURE 5. SURGE DECAY, 11.4 m/s CONSTANT WIND. PLATFORM SURGE VELOCITY (TOP) AND BLADE PITCH ANGLE (BOTTOM)

The surge damping is presented in Fig. 6. As shown, the damping for the case with rated wind decreases to zero as the limit cycle is reached.

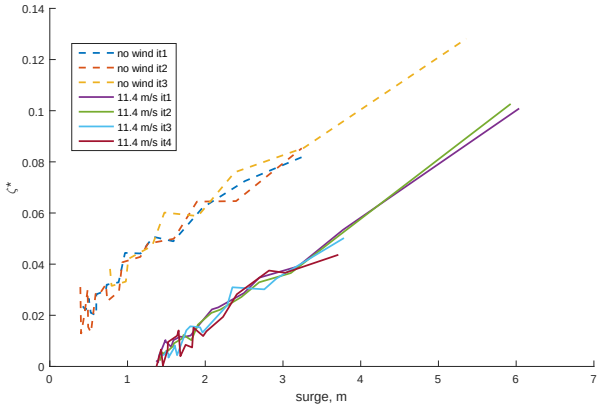

FIGURE 6. SURGE DAMPING, 11.4 m/s CONSTANT WIND

Three pitch decays at 11.4 m/s were also carried out, as shown in Fig. 7. The pitch natural period increased significantly with the operational turbine at rated speed, and the decay is slightly slower. Although the modified pitch period is lower than the control natural period, the wind turbine controller does not respond immediately, and the system remains stable in pitch. As shown in Fig. 7, the controller is slightly behind the platform pitch due to the proximity of the controller frequency and the platform pitch frequency.

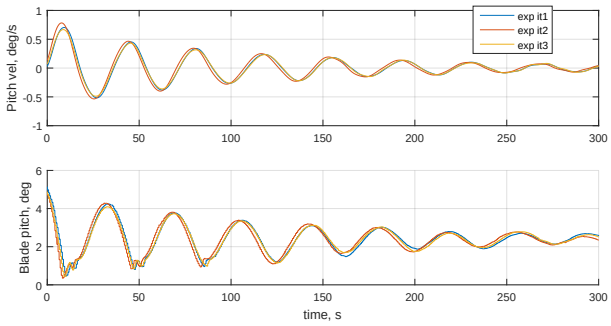

FIGURE 7. PITCH DECAY, 11.4 m/s CONSTANT WIND. PLATFORM PITCH VELOCITY (TOP) AND BLADE PITCH ANGLE (BOTTOM)

The damping in pitch at rated speed remains at a level similar to the case with no wind.

Decay tests above rated wind speed

Four surge decay tests and four pitch decay tests were carried out at above rated wind speed, as shown in Fig. 8 and 9.

Although the wind turbine blade pitch controller is active at above-rated wind speeds, the negative feedback is smaller at 20 m/s than at 11.4 m/s due to gain scheduling. In Fig. 8, the surge velocity and blade pitch angle are shown. Due to gain scheduling, the same variation in rotor speed results in smaller changes in the blade pitch angle as the blade pitch angle increases. In this case the mean blade pitch angle is above 17 degrees. Due to the small changes in the blade pitch angle, the hydrodynamic damping is sufficient to result in decay despite some negative feedback from the controller. There is a slight decrease in surge damping with above-rated wind compared to the case without wind, but the difference is small.

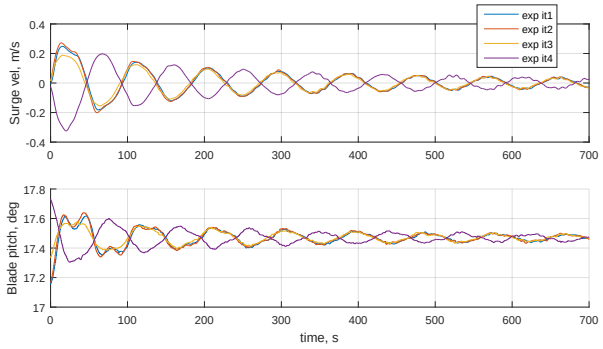

FIGURE 8. SURGE DECAY, 20 m/s CONSTANT WIND. PLATFORM SURGE VELOCITY (TOP) AND BLADE PITCH ANGLE (BOTTOM)

The pitch natural period increased significantly with the operational turbine at rated speed. The damping is slightly higher for the 20 m/s wind speed than for the case without wind. As in the surge decay test at 20 m/s, the variation in the blade pitch angle is small. The effect of the delay between the pitch control response and the pitch velocity results in the presence of some aerodynamic damping in the system.

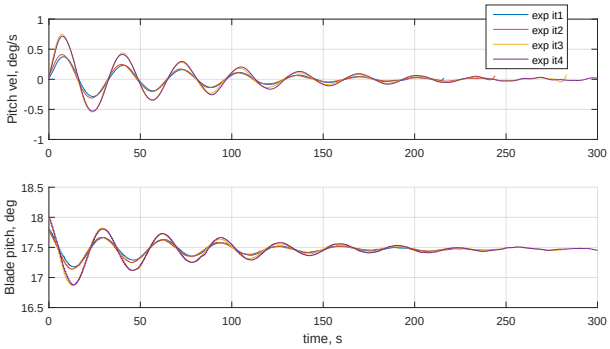

FIGURE 9. PITCH DECAY, 20 m/s CONSTANT WIND. PLATFORM PITCH VELOCITY (TOP) AND BLADE PITCH ANGLE (BOTTOM)

REGULAR AND PINK WAVE TESTS

Regular wave tests with 1/60 steepness were carried out for three periods (8, 11, and 16 seconds) and three wave headings (0, 60, and 90 degrees) without the hybrid system present. Regular wave tests for 8 and 11 second wave periods at 0 degree wave heading were also carried out with the hybrid system present: without wind, with constant wind at 8 m/s, and with constant wind at 15 m/s. Analysis of the regular waves is carried out for 10-15 wave periods after the initial ramp. As far as possible, the analysis is carried out before the wave reflections from the beach reached the model. Pink noise tests, with an irregular wave spectrum which is ideally constant over a range of frequencies and zero outside that range, were also carried out in order to examine the wave-only response over a wider range of frequencies. The pink noise tests, which are summarized in Table 12, were carried out without the hybrid system.

Response amplitude operators (RAOs) can be computed based on the measured waves and responses in pink noise and in regular waves. Fig. 10 shows the surge, heave, and pitch RAOs for the waves from zero degrees. In addition to the results from the two pink noise tests without the hybrid system present, the results from the regular wave tests with (including pretension, see Part I [1]) and without the hybrid system, and with constant wind, are included. The motions appear to behave quite linearly

TABLE 12. PINK WAVE TESTS (NO WIND)

H_s (m)	T (s)	β (deg)
2.0	3.5-22.0	0
4.0	4.5-22.0	0
4.0	4.5-16.0	60
4.0	4.6-16.0	90

with respect to the significant wave height in the pink noise tests, and the regular wave results are in good agreement with the pink noise results. The motion amplitudes are not significantly affected by the hybrid system or by the aerodynamic effects in constant wind.

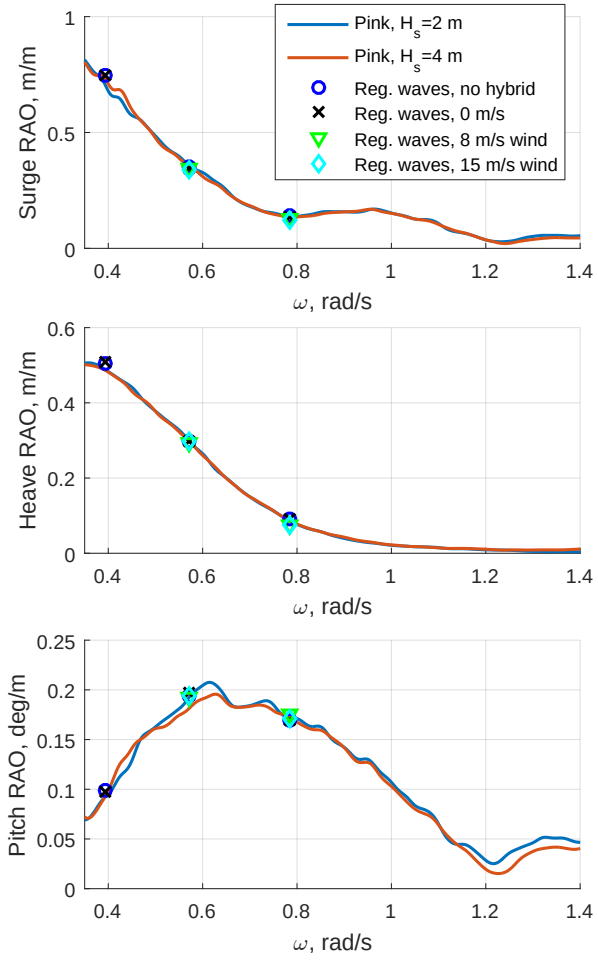

FIGURE 10. MOTION RAOs, 0 DEG WAVE HEADING

Similarly, the RAOs for the bending moments at the base of the tower and at the base of column 3 are shown together with the regular wave results in 0 degree wave heading in Fig. 11. Linear behavior is observed, and there is good agreement between the regular wave tests without wind (with and without the hybrid system) and the pink noise tests. The aerodynamic forces are observed to have some effect on the amplitude of the moment, particularly for column 3. This effect is likely related to the mean pitch angle of the platform, which affects the geometry of the column with respect to the waves.

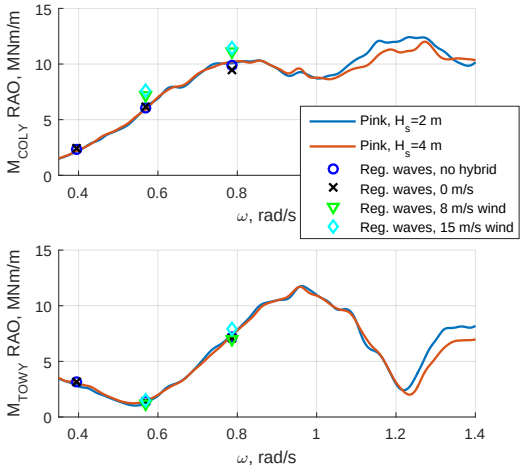

FIGURE 11. MOMENT RAOs OF COLUMN 3 AND TOWER BASE, 0 DEG WAVE HEADING

IRREGULAR WAVE AND TURBULENT WIND TESTS

In total, 9 tests were carried out with irregular waves and turbulent wind, and 3 tests were carried out with irregular waves and no wind, as summarized in Table 13. In Table 13, the wind and wave directions are 0 degrees and the current is turned off unless otherwise indicated in the comments.

One wind speed below rated, one speed near rated, and one wind speed above rated (near cut-out) were considered. The test matrix includes repetition tests in both wind-wave conditions and wind-wave-current conditions. The majority of the tests were carried out with aligned wind and waves coming from the x direction, while one test included waves from 60 degrees. The majority of the tests were carried out with the wind turbine operating, with two tests examining the effects of wind turbine control fault.

The effective duration of each irregular wave test corresponds to three (3) hours full scale. A sufficient lapse of time was used between tests to avoid wave distortion from the previous test.

The wind input was generated in 64-bit TurbSim v1.5 [23]. The turbulent wind files were generated for 28 x 28 grids in the

y-z plane, corresponding to 160 m x 160 m centered at a height of 90 m above the still water line. The time step in the wind files was 0.22 s and each time series lasted 12500 s (corresponding to 3 hours of full scale time, plus approximately 5 min extra model scale time). There was no vertical shear in the wind files. The normal turbulence model (NTM) for class B wind turbines was used, and the Kaimal wind spectrum was applied. The relatively low resolution of the wind file is related to the frequencies of interest in the present test and hardware (memory) limitations, but these limitations are not inherent to the test methodology. Additional discussion of the wind field frequencies can be found in [1].

TABLE 13. IRREGULAR WAVE TESTS. SPECIFIED/OBTAINED VALUES ARE SHOWN FOR H_s and T_p.

H_s (m)	T_p (s)	U (m/s)	I (%)	Comment
15.3/15.11	14.0/13.86	0		w/out hybrid system
3.6/3.62	10.2/10.13	0		w/ and w/out hybrid system
5.9/5.86	11.3/11.05	25	13.2	repeated
5.9/5.86	11.3/11.21	25	13.2	60 deg wave
3.6/3.62	10.2/10.13	11	17.0	
5.2/4.99	8.0/8.02	8	19.5	
5.9/5.26	11.3/11.05	25	13.2	current 1.12 m/s, repeated
5.9/5.86	11.3/11.05	25	13.2	Shutdown, blade seize

The two tests with H_s =5.9 m, T_p =11.3 s, and turbulent wind (U =25 m/s) can be used to examine the repeatability of the wind-wave tests. The platform motions over a short time duration are compared in Fig. 12.

There is less than 2 % difference in the statistical results between the two tests, which suggests good repeatability.

Fig. 13 shows time series of the platform motions in combined, wave-only, and wind-only conditions. The mean value of the responses is subtracted in order to see the dynamic components more clearly. Visually, Fig. 13 shows that the low-frequency motions are primarily excited by the wind, and that the wave-frequency responses are fairly independent from the low-frequency motions.

The low- and wave-frequency parts of the motion spectra for the wind-wave, wave-only, and wind-only surge, heave, and pitch motions are shown separately in Figs. 14 and 15. Based on Fig. 14, for the surge motion, the presence of waves tends to decrease the low-frequency response. This is consistent with the fact that the wave-frequency motions contribute non-linearly to the rotor thrust [24, 25].

The low-frequency (natural frequency) heave response is largest in the wave-only condition and is somewhat dampened

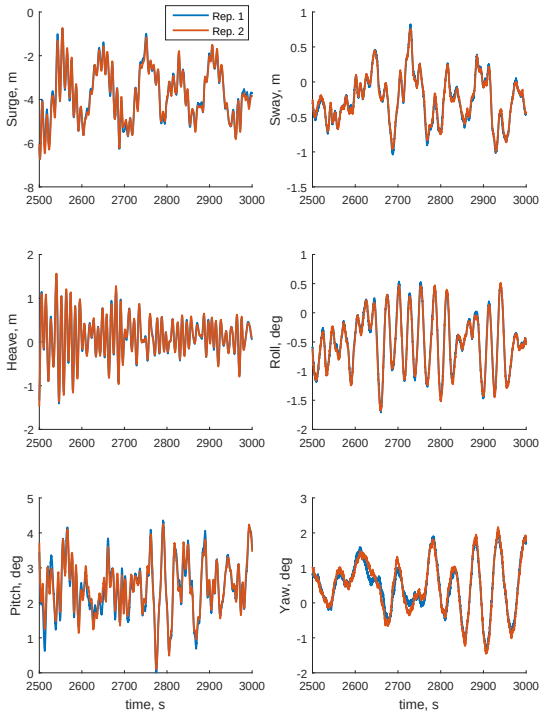

FIGURE 12. REPEATED TESTS, IRREGULAR WAVES AND TURBULENT WIND, H_s =5.9 m, T_p =11.3 s, U =25 m/s.

when the wind is also present. There is little wind-wave coupling for the low-frequency pitch motions. Fig. 15 suggests that there is very little influence from the wind on the wave-frequency motions for this platform.

Time series of the column and tower base bending moments in wind-wave, wave-only, and wind-only conditions are shown in Fig. 16. The low-frequency wind-induced effects on the column are small, as expected. As a result of the changed mean position/orientation of the column due to wind forces, the amplitude of the wave-frequency column bending moment is larger for the wind-wave condition than the wave-only condition.

The tower base bending moment shows significant variation in both the low-frequency and wave-frequency regions, but there is little influence of the waves on the low-frequency tower base bending moment variation, and little influence of the wind on the wave-frequency variation.

The low-frequency component of the mooring line tensions, which is largely dictated by the surge motions, is dominated by wind excitation. The presence of waves dampens the low-frequency surge motion somewhat, and there is a corresponding decrease in the low-frequency mooring forces for the wind-wave case compared to the wind-only case. The wave-frequency variation in the mooring line forces depends on the mean position of the platform. As such, the wave-frequency mooring line force

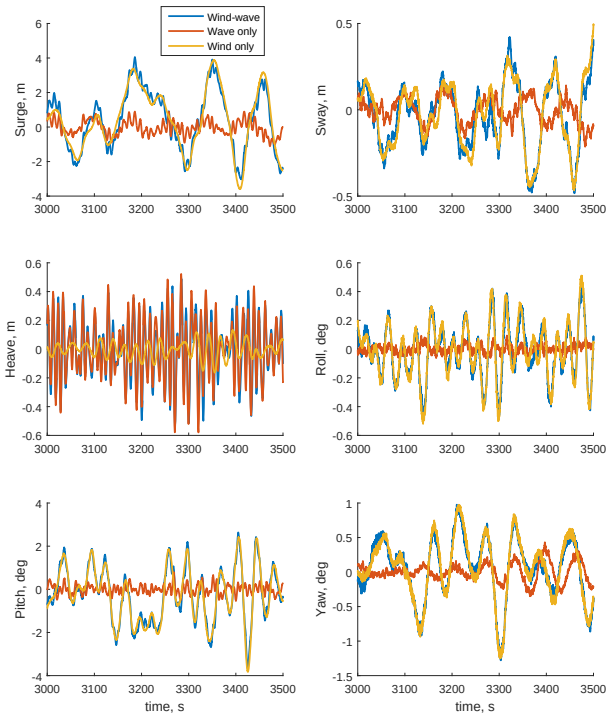

FIGURE 13. PLATFORM MOTIONS IN WIND-WAVE,WAVE-ONLY, AND WIND-ONLY CONDITIONS. H_s =3.6 m, T_p =10.2 s, U =11 m/s. MEAN VALUES ARE REMOVED.

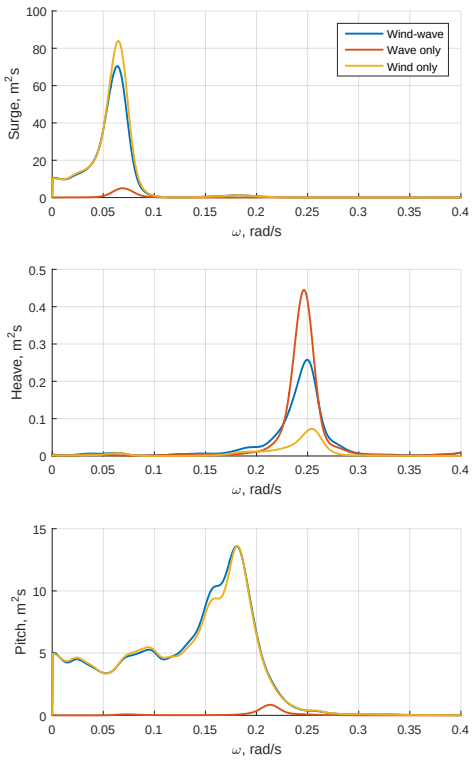

FIGURE 14. LOW-FREQUENCY PART OF PLATFORM MOTION SPECTRA. WIND-WAVE, WAVE-ONLY, AND WIND-ONLY CONDITIONS. H_s =3.6 m, T_p =10.2 s, U =11 m/s.

variation increases for lines 1 and 2 (upwind) in the wind-wave case, while the variation decreases for line 3 (downwind).

The key statistics for the wind-wave test near rated wind speed are compared to the wave-only and wind-only statistics in Table 14. Table 14 also includes the results from superposition in the time domain (direct addition of the time series from 4330 and 1713). In general, direct superposition of the time series gives slightly conservative results for the platform motions and mooring line tensions, but is not conservative for the bending moments in the column. Superposition of the statistics tends to give slightly larger errors.

CONCLUSIONS

ReaTHM^{TM} testing of a semi-submersible wind turbine was carried out at the MARINTEK Ocean Basin as a part of the NOWITECH research center. Physically modelled waves and current were applied to the model, while aerodynamic and generator loads on the wind turbine were applied by actuators based on real-time simulations (accounting for the measured motions).

Extensive identification tests were carried out, and the wind turbine (including the control system) was found to have significant effects on the natural periods and damping of the system.

The tested conditions permitted a detailed examination of the motions, mooring line forces, and tower and column bending moments in severe waves, aligned wind and waves, misaligned wind and waves, wind-wave-current, and in several wind turbine fault conditions. For this platform, interaction between the aerodynamic and hydrodynamic loads was observed primarily at low frequencies.

ACKNOWLEDGMENT

The authors gratefully acknowledge the financial support from the Research Council of Norway granted through the Norwegian Research Centre for Offshore Wind Technology (NOWITECH).

REFERENCES

[1] Sauder, T., Chabaud, V., Thys, M., Bachynski, E. E., and Sæther, L. O., 2016. "Real-time hybrid model testing of a braceless semi-submersible wind turbine: Part I: The hybrid approach". In 35th International Conference on Ocean, Offshore and Arctic Engineering, no. OMAE2016-54435.

TABLE 14. Comparison of key responses: wind-wave, wave-only, wind-only

	Wind and waves 4310	Wave-only 4330	Wind-only 1713 and 1720	Superposition in time domain	Deviation (%) from superposition
Std. Dev. Surge (m)	1.59	0.44	1.66	1.69	-5.94
Mean Surge (m)	-8.09	-0.12	-7.91	-7.97	1.49
Std. Dev. Heave (m)	0.21	0.22	0.07	0.22	-5.42
Std. Dev. Roll (deg)	0.17	0.03	0.17	0.17	-1.60
Std. Dev. Pitch (deg)	1.19	0.23	1.18	1.18	0.56
Mean Pitch (deg)	5.77	-0.32	5.74	5.44	5.73
Std. Dev. Yaw (deg)	0.49	0.09	0.52	0.52	-6.01
Std. Dev. M_{COLY} (MNm)	10.23	7.85	2.39	8.20	19.85
Mean M_{COLY} (MNm)	-8.70	0.55	-8.81	-8.27	4.97
Std. Dev. M_{TOWY} (MNm)	15.34	6.26	14.10	15.29	0.33
Mean M_{TOWY} (MNm)	85.22	-5.85	85.01	79.44	6.79
Std. Dev. F_{MOOR1} (kN)	63.25	18.01	64.75	66.17	-4.62
Std. Dev. F_{MOOR2} (kN)	62.42	19.85	62.84	65.27	-4.57
Std. Dev. F_{MOOR3} (kN)	64.38	29.59	67.84	72.00	-11.84

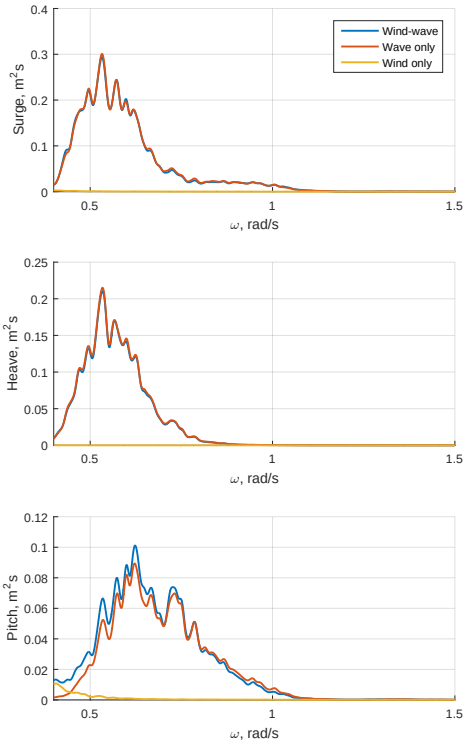

FIGURE 15. WAVE-FREQUENCY PART OF PLATFORM MOTION SPECTRA. WIND-WAVE, WAVE-ONLY, AND WIND-ONLY CONDITIONS. H_s =3.6 m, T_p =10.2 s, U =11 m/s.

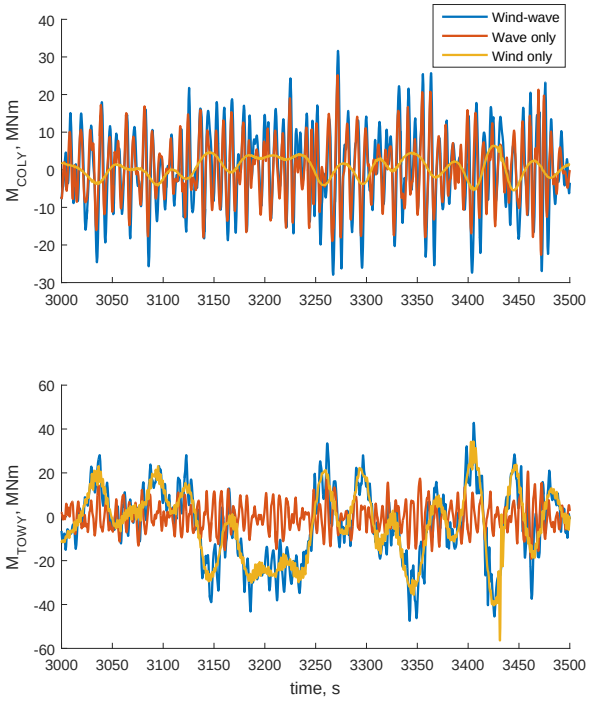

FIGURE 16. TOWER AND COLUMN BENDING MOMENTS IN WIND-WAVE, WAVE-ONLY, AND WIND-ONLY CONDITIONS. H_s =3.6 m, T_p =10.2 s, U =11 m/s. MEAN VALUES ARE REMOVED.

[2] IEA Wind Task 30, 2012. Experts' meeting on computer code validation for offshore wind system modeling. Tech. rep., IEA Wind.

[3] Robertson, A. N., Jonkman, J., Goupee, A. J., Coulling, A. J., Prowell, I., Browning, J., Masciola, M. D., and Molta, P., 2013. "Summary of conclusions and recommendations drawn from the DeepCwind scaled floating offshore wind system test campaign". In Proceedings of the ASME

2013 32nd International Conference on Ocean, Offshore and Arctic Engineering, no. OMAE2013-10817.

[4] Courbois, A., Flamand, O., Toularastel, J.-L., Ferrant, P., and Rousset, J.-M., 2013. "Applying relevant wind generation techniques to the case of floating wind turbines". In European-African Conference on Wind Engineering (EACWE).

[5] Newton, J. M., Cameron, M. P., Urbina, R., Kimball, R. W., Goupee, A. J., and Thiagarajan, K. P., 2015. "Characteriszation of a wind tunnel for use in offshore wind turbine development". In 34th International Conference on Ocean, Offshore and Arctic Engineering, no. OMAE2015-41979.

[6] Roddier, D., Cermelli, C., Aubault, A., and Weinstein, A., 2010. "WindFloat: A floating foundation for offshore wind turbines". *Journal of Renewable and Sustainable Energy,* ***2***(3), p. 033104.

[7] Wan, L., Gao, Z., and Moan, T., 2015. "Experimental and numerical study of hydrodynamic responses of a combined wind and wave energy converter concept in survival modes". *Coastal Engineering,* ***104***, pp. 151 – 169.

[8] Fowler, M. J., Kimball, R. W., Thomas, D. A., and Goupee, A. J., 2013. "Design and testing of scale model wind turbines for use in wind/wave basin model tests of floating offshore wind turbines". In 32nd International Conference on Ocean, Offshore and Arctic Engineering, no. OMAE2013-10122.

[9] Kimball, R., Goupee, A. J., Fowler, M. J., de Ridder, E.-J., and Helder, J., 2014. "Wind/wave basin verification of a performance-matched scale-model wind turbine on a floating offshore wind turbine platform". In Proceedings of the ASME 2014 33rd International Conference on Ocean, Offshore and Arctic Engineering, no. OMAE2014-24166.

[10] Bottasso, C. L., Campagnolo, F., and Pectrović, V., 2014. "Wind tunnel tetsting of scaled wind turbine models: Beyond aerodynamics". *Journal of Wind Engineering and Industrial Aerodynamics,* ***127***, pp. 11–28.

[11] Fernandes, G., Make, M., Gueydon, S., and Vaz, G., 2014. "Sensitivity to aerodynamic forces for the accurate modelling of floating offshore wind turbines". In RENEW2014, G. Soares, ed., no. ISBN: 978-1-138-02871-5.

[12] Azcona, J., Bouchotrouch, F., González, M., Garciandía, J., Munduate, X., Kelberlau, F., and Nygaard, T. A., 2014. "Aerodynamic thrust modelling in wave tank tests of offshore floating wind turbines using a ducted fan". *Journal of Physics: Conference Series,* ***524***, Jun, pp. 1–11.

[13] Hall, M., Moreno, J., and Thiagarajan, K., 2014. "Performance specifications for real-time hybrid testing of 1:50-scale floating wind turbine models". In Proceedings of the ASME 2014 33rd International Conference on Ocean, Offshore and Arctic Engineering OMAE2014, no. OMAE2014-24497.

[14] Chabaud, V., Steen, S., and Skjetne, R., 2013. "Real-time hybrid testing for marine structures: Challenges and strategies". In 32nd International Conference on Ocean, Offshore and Arctic Engineering, no. OMAE2013-10277.

[15] Berthelsen, P. A., Bachynski, E. E., Karimirad, M., and Thys, M., 2016. "Real-time hybrid model testing of a braceless semi-submersible wind turbine. Part III: Calibration of a numerical model". In 35th International Conference on Ocean, Offshore and Arctic Engineering, no. OMAE2016-54640.

[16] Luan, C., Gao, Z., and Moan, T., 2016. "Design and analysis of a braceless steel 5-mw semi-submersible wind turbine". In 35th International Conference on Ocean, Offshore and Arctic Engineering, no. OMAE2016-54848. (submitted for publication).

[17] Jonkman, J., Butterfield, S., Musial, W., and Scott, G., 2009. Definition of a 5-MW reference wind turbine for offshore system development. Tech. Rep. NREL/TP-500-38060, National Renewable Energy Laboratory, February.

[18] Jonkman, J., 2010. Definition of the floating system for Phase IV of OC3. Tech. Rep. NREL/TLP-500-47535.

[19] Jonkman, B. J., and Jonkman, J. M., 2010. Documentation of updates to FAST, A2AD, and AeroDyn: Released March 31, 2010, including the revised AeroDyn interface. Tech. rep.

[20] Moriarty, P. J., and Hansen, A. C., 2005. AeroDyn theory manual. Tech. Rep. NREL/TP-500-36881.

[21] Laino, D. J., Hansen, A. C., and Minnema, J. E., 2002. "Validation of the AeroDyn subroutines using NREL unsteady aerodynamics experiment data". *Wind Energy,* ***5***, pp. 227–244.

[22] Larsen, T. J., and Hanson, T. D., 2007. "A method to avoid negative damped low frequent tower vibrations for a floating, pitch controlled wind turbine". *Journal of Physics: Conference Series, The Second Conference on The Science of Making Torque from Wind,* ***75***.

[23] Jonkman, B., 2009. TurbSim user's guide: Version 1.50. Tech. Rep. NREL/TP-500-46198, National Renewable Energy Laboratory, September.

[24] Bachynski, E. E., Kvittem, M. I., Luan, C., and Moan, T., 2014. "Wind-wave misalignment effects on floating wind turbines: motions and tower load effects". *Journal of Offshore Mechanics and Arctic Engineering,* ***136***, pp. 041902–1–041902–12.

[25] Kvittem, M. I., 2014. "Modelling and response analysis for fatigue design of a semi-submersible wind turbine". PhD thesis, Norwegian University of Science and Technology.